

# Application of STATCOM-supercapacitor for low-voltage ride-through capability in DFIG-based wind farm

M. K. Döşoğlu<sup>1</sup> · A. Basa Arsoy<sup>2</sup> · U. Güvenç<sup>1</sup>

Received: 7 December 2015 / Accepted: 19 January 2016 / Published online: 3 February 2016  
© The Natural Computing Applications Forum 2016

**Abstract** Low-voltage problem emerges in cases of symmetrical and asymmetrical fault in power systems. This problem can be solved out by ensuring low-voltage ride-through capability of wind power plants, through a static synchronous compensator (STATCOM). The purpose of this study is to reveal that the system can be recovered well by inserting a STATCOM with energy storage to a bus where a double-fed induction generator (DFIG)-based wind farm has been connected, so the bus voltage is maintained within desired limits during a fault. Moreover, a supercapacitor is used as an energy storage element. Modeling of the DFIG and STATCOM along with the nonlinear supercapacitor was carried out in a MATLAB/Simulink environment. The behaviors of the system under three- and two-phase faults have been compared with and without STATCOM-supercapacitor, by observing the parameters of DFIG output voltage, active power, speed, electrical torque variations, and d–q axis stator current variations. It was found that the system became stable in a short time when the STATCOM-supercapacitor was incorporated into the full-order modeled DFIG.

**Keywords** Doubly fed induction generator (DFIG) · Static synchronous compensator (STATCOM) · Supercapacitor · Symmetric and asymmetric fault

## 1 Introduction

Tendency toward renewable energy has increased recently as a result of increase in price of fossil fuels and restriction in their use. The most important one of them is wind energy. Grid-connected operation of wind farms used in converting wind energy into electrical energy has become popular. Today, the innovative concepts of wind turbines are provided with technologies for not only generators but also power electronics. Modern wind farms have the different operation point and a grid connection by power converters. Modern wind farms have a more widespread in the market national or international. Modern wind farms are known as the DFIG [1]. However, grid-connected wind power plants can be exposed to some problems [2–4]. LVRT is the most important one and can be developed by using in STATCOM.

In the literature, several studies on STATCOM have been carried out. STATCOM is recommended for power system voltage stability in [5, 6]. Modeling of STATCOM is given for power flow and voltage stability analysis along with voltage and phase control. The STATCOM-decoupled operation shows that a DFIG works as an induction generator while the grid-/rotor-side converter units work as a reactive power source in transient state. The power characteristics of the DFIG have been enhanced by the maximum capability of the STATCOM, based on different operating conditions strategy [7–10]. The level of voltage dips besides the over-currents in the DFIG are substantially reduced by this operation during grid faults, thereby enhancing the LVRT capability of the wind farm considerably. In addition, this control unit develops as a different controller method for the wind farm, in this way, provides of the system by using the STATCOM during faults [11–13].

---

✉ M. K. Döşoğlu  
kenandosoglu@duzce.edu.tr

<sup>1</sup> Faculty of Technology, Department of Electrical-Electronics Engineering, University of Düzce, Konuralp Campus, 81620 Düzce, Turkey

<sup>2</sup> Faculty of Engineering, Department of Electrical Engineering, University of Kocaeli, Umuttepe Campus, 41380 Kocaeli, Turkey

The impact of a STATCOM on the connection of a large wind farm to a power system was studied in [14, 15]. Particularly, the weak power systems which have two large wind farms are presented. Issues of power quality are stressed, and a central STATCOM was utilized to solve such issues, in particular, the short-term voltage flicker and fluctuations. The transient stability margin has been defined in introducing of LVRT capability in DFIG. A simple a new method based on moment-slip characteristics can be used to measure the effect of the STATCOM during transient stability [16]. Multi-variable controller has been proposed in enhancing the LVRT capability of DFIG-based wind farms as given in [17, 18]. The designed multi-variable controller enables suitable post-fault performance for both small and large perturbations. In Ref [19] there is a discussion on the use of trajectory sensitivity analysis (TSA) in estimating the transient stability point of a DFIG-based wind farm compensated by a STATCOM device. The eligibility for the optimal placement of the STATCOM for fault conditions has also been observed in [20, 21] in which the results of utilizing a STATCOM to improve damping oscillation of an offshore-based wind farm are given. The performance of the offshore-based wind farm in question is simulated by an equivalent aggregated DFIG driven by an equivalent aggregated wind turbine, and the DFIG grid/rotor-side converters have been studied for subsynchronous resonance mitigation [22]. The issues of the design of auxiliary subsynchronous resonance and determination of control input–output signals, and locus approach have also been covered in the same study. Besides, power oscillation damping (POD) is important for regulation of voltage sags/swells apart from the over-currents in the DFIG-based wind farm in grid faults and hence significantly develops the LVRT capability of the DFIG-based wind farm [23–25].

This paper differs from other papers in the literature by the way of modeling of a supercapacitor-type ESS and a wind turbine generator for LVRT applications. Nonlinear modeling of a STATCOM-supercapacitor which is based on a voltage–capacity relationship is conducted in this study. Thanks to using lookup table in voltage–capacity relationship, supercapacitor provides a better dynamic response than various papers in the literature. Mathematical equations for modeling are presented and implemented on a test system using MATLAB/Simulink. A comparison is drawn between the states having a DFIG with/without a STATCOM-supercapacitor both in three-phase fault analysis and two-phase fault. The study results show that the system becomes stable in a short time, and power oscillations decreases when a STATCOM-supercapacitor ESS is coupled to a DFIG during transient states.

## 2 Modeling of wind farm

The DFIG consist of grid-side converter, rotor-side converter, and crowbar units, in which the rotor-side converter and grid-side converter are integrated to a DC bus. A rotor-side converter and a grid-side converter along with their controllers in both steady-state and transient conditions have a controlling role in the operation of the DFIG. The rotor voltage is controlled by those converters in magnitude and phase angle, making them useful for power control [26–28].

The mechanical power acquired from the wind speed, which is generated due to the wind, the blade tip speed ratio and the blade pitch angle, is expressed by the rotor model, as demonstrated in the following equation.

$$P_w = \frac{1}{2} \rho A u^3 C_p(\lambda, \theta) \quad (1)$$

where  $P_w$  is the mechanical power acquired by the wind turbine rotor,  $\rho$  is the air density,  $A$  is the area of the rotor disk,  $u$  is the wind speed, and  $C_p$  is the power coefficient. The power coefficient derivation from term tip speed ratio  $\lambda$  and the pitch angle of the rotor blades  $\theta$ . The speed ratio is described as the ratio not only the blade tip speed but the wind speed, explained as,

$$\lambda = \frac{w_r R}{u} \quad (2)$$

where  $w_r$  is the rotor speed and  $R$  is the radius of the wind turbine rotor. The optimum power acquired is given in Eq. (3).

$$P_{op} = K_{op} w_r^2 \quad (3)$$

The drive trains of DFIG wind turbine with two masses are defined in Eqs. (4) and (5)

$$T_w - T_m = 2H \frac{dw_r}{dt} \quad (4)$$

$$T_m = D_m(w_r - w) + K_m \int (w_r - w) dt \quad (5)$$

where  $T_w$  is the mechanical torque in rotor,  $T_m$  is the mechanical torque in generator,  $H$  is the rotor inertia, and  $K_m$  and  $D_m$  are the stiffness and damping of mechanical [29].

The DFIG model is given by generator's variables equations in the d–q synchronous reference frame [30]. D–q axes stator and rotor voltages, electrical torque, and d–q axes linkage fluxes are shown in Eqs. (6) and (14).

$$v_{ds} = R_s i_{ds} + w_s \lambda_{qs} + \frac{d}{dt} \lambda_{ds} \quad (6)$$

$$v_{qs} = R_s i_{qs} - w_s \lambda_{ds} + \frac{d}{dt} \lambda_{qs} \quad (7)$$

$$v_{dr} = R_r i_{dr} - sw_s \lambda_{qr} + \frac{d}{dt} \lambda_{dr} \tag{8}$$

$$v_{qr} = R_r i_{qr} + sw_s \lambda_{dr} + \frac{d}{dt} \lambda_{qr} \tag{9}$$

$$M = \lambda_{ds} i_{qs} - \lambda_{qs} i_{ds} \tag{10}$$

$$\lambda_{ds} = (L_s + L_m) i_{ds} + L_m i_{dr} \tag{11}$$

$$\lambda_{qs} = (L_s + L_m) i_{qs} + L_m i_{qr} \tag{12}$$

$$\lambda_{dr} = (L_m + L_r) i_{dr} + L_m i_{ds} \tag{13}$$

$$\lambda_{qr} = (L_r + L_m) i_{qr} + L_m i_{qs} \tag{14}$$

In these equations,  $v_{ds}, v_{dr}, v_{qs}, v_{qr}$ :  $d$  and  $q$  axis voltages of stator and rotor,  $i_{ds}, i_{dr}, i_{qs}, i_{qr}$ :  $d$  and  $q$  axis of currents of stator and rotor,  $\lambda_{ds}, \lambda_{qs}, \lambda_{dr}, \lambda_{qr}$ :  $d$  and  $q$  axis magnetic fluxes of stator and rotor,  $w_s$ : angular speed of stator,  $s$ : slip,  $R_s$  and  $R_r$ : resistance of stator and rotor,  $L_s$  and  $L_r$ : inductance of stator and rotor,  $L_m$ : magnetic inductance and  $M$ : torque [31, 32].

The rotor-side converter controls the output active power the DFIG. The active power and voltage equations are shown  $v_{dr}$  and  $v_{qr}$ , respectively.  $x_1, x_2, x_3, x_4$  control equations are shown between Eqs. (15) and (22)

$$\frac{dx_1}{dt} = P_{ref} + P_s \tag{15}$$

$$I_{qr\_ref} = K_{p1}(P_{ref} + P_s) + K_{i1}x_1 \tag{16}$$

$$\frac{dx_2}{dt} = I_{qr\_ref} - I_{qr} = K_{p1}(P_{ref} + P_s) + K_{i1}x_1 - I_{qr} \tag{17}$$

$$\frac{dx_3}{dt} = v_{s\_ref} - v_s \tag{18}$$

$$I_{dr\_ref} = K_{p3}(v_{s\_ref} - v_s) + K_{i3}x_3 \tag{19}$$

$$\frac{dx_4}{dt} = I_{dr\_ref} - I_{dr} = K_{p3}(v_{s\_ref} - v_s) + K_{i3}x_3 - I_{dr} \tag{20}$$

$$v_{qr} = K_{p2}(K_{p1}\Delta P + K_{i1}x_1 - I_{qr}) + K_{i2}x_2 + sw_s L_m I_{ds} + sw_s L_{rr} I_{qr} \tag{21}$$

$$v_{dr} = K_{p2}(K_{p3}\Delta v + K_{i3}x_3 - I_{dr}) + K_{i2}x_4 - sw_s L_m I_{qs} - sw_s L_{rr} I_{dr} \tag{22}$$

where  $K_{p1}$  proportional power arrange,  $K_{i1}$  integrating power arrange,  $K_{p2}$  proportional rotor-side converter current arrange and  $K_{i2}$  rotor-side converter current arrange,  $K_{p3}$  proportional grid-side voltage arrange,  $K_{i3}$  integrating grid-side voltage arrange,  $I_{dr\_ref1}$   $d$  axis current reference,  $I_{qr\_ref1}$   $q$  axis current reference,  $v_{s\_ref1}$  specified terminal voltage reference;  $P_{ref1}$  active power reference.

The grid-side converter provides control for both the DC link unit and the terminal of reactive power.  $x_5, x_6,$  and  $x_7$  control equations are shown Eqs. (23) and (28)

$$\frac{dx_5}{dt} = V_{dc\_ref} - V_{dc} \tag{23}$$

$$I_{dgrid\_ref} = -K_{pdgrid}\Delta v_{dc} + K_{1dgrid}x_5 \tag{24}$$

$$\frac{dx_6}{dt} = I_{dgrid\_ref} - I_{dgrid} = -K_{pdgrid}\Delta v_{dc} + K_{1dgrid}x_5 - I_{dgrid} \tag{25}$$

$$\frac{dx_7}{dt} = I_{qgrid\_ref} - I_{qgrid} \tag{26}$$

$$\begin{aligned} \Delta v_{dgrid} &= K_{pgrid} \frac{dx_6}{dt} + K_{igrid}x_6 \\ &= K_{pgrid}(-K_{pdgrid}\Delta v_{dc} + K_{1dgrid}x_5 - I_{dgrid}) + K_{1grid}x_6 \end{aligned} \tag{27}$$

$$\begin{aligned} \Delta v_{qgrid} &= K_{pgrid} \frac{dx_7}{dt} + K_{igrid}x_7 \\ &= K_{pgrid}(I_{qgrid\_ref} - I_{qgrid}) + K_{1grid}x_7 \end{aligned} \tag{28}$$

where  $K_{pqgrid}$  proportional the DC link voltage arrange,  $K_{idgrid}$  integrating the DC link voltage arrange,  $K_{pgrid}$  proportional grid-side converter current arrange,  $K_{i2}$  integrating grid-side converter current arrange,  $K_{igrid}$  proportional the grid-side converter current arrange,  $V_{dc\_ref1}$  reference of the DC link voltage,  $I_{qgrid}$   $q$  axis the grid-side converter current reference [31].

### 3 Wind energy and energy storage

Energy storage system devices should be made more commercially viable for the operation of the generator because storage system is important both for grid and wind farm based on DFIG during transient cases [33, 34]. In addition, storage should be preferred in power control as well as power dispatch, energy management, and power quality.

Wind farm can be used in storage and suboptimal power points for power dispatch. These two ways ensure a reliable operation of DFIG. Whereas storage systems can influence any operation points, suboptimal power point can influence only certain operation points. While storage systems can increase efficiency, they can also improve LVRT capability during transient cases.

Storage systems cannot be used in wind farm for some conditions particularly when there is a difference between set power point and the terminal generator. The operating point of DFIG can vary in different conditions. Regulating the set power point and terminal of DFIG, storage system devices provide energy management under various transient operations. Besides, they extend operation by tracking the power reference in storage limitation [35].

The selection of grid configuration relies on the utility distribution or transmission level. The selection of grid configuration is performed both in strong grid and in weak grid considering power quality issues [36].

### 4 STATCOM-supercapacitor modeling

The STATCOM-supercapacitor integrated to the generator terminals is shown in Fig. 1.

There are two tasks performed by the STATCOM; namely, keeping up with the short-term reactive power require of the system and of the supercapacitor [37]. DC–DC buck–boost converter was used in connecting the supercapacitor to the STATCOM. In controlling the operation of the converters, the duty ratio is differentiated through switches. Variable components  $I_n$  in DC–DC converter circuit are calculated through  $R_{sc}$ . The STATCOM current and voltage equations are given in Eq. (29).

$$L_{st} \frac{dI_{st}}{dt} + R_{st}I_{st} = V_{st} - V_s \tag{29}$$

where  $V_{st} = mV_{dc}\angle\psi + \theta_s$ ,  $V_s = V_s\angle\theta_s$ ,  $V_{dc}$  is the STATCOM DC link voltage;  $m$  and  $\psi$  are the modulation index and the STATCOM phase angle. STATCOM d–q axes currents are given in Eqs. (30) and (31).

$$I_{std} = \frac{wR_{st}}{L_{st}}I_{std} + \frac{w_e}{w}I_{stq} + \frac{w}{L_{st}}mV_{dc} \cos(\psi + \theta) - v_{sd} \tag{30}$$

$$I_{stq} = -\frac{w_e}{w}I_{std} - \frac{wR_{st}}{L_{st}}I_{stq} + \frac{w}{L_{st}}mV_{dc} \sin(\psi + \theta) - v_{sq} \tag{31}$$

Given that the converter is not loss, the power regulate equation gives rise to the capacitor voltage equation,

$$\frac{dV_{dcs}}{dt} = -\frac{m}{C_{dcs}}(I_{std} \cos(\psi + \theta) + I_{stq} \sin(\psi + \theta)) - \frac{I_{sc}}{C_{dcs}} \tag{32}$$

where  $I_{sc}$  and  $C_{dcs}$  are the supercapacitor current and the DC link capacitance, respectively. The supercapacitor current is involved in the supercapacitor voltage  $V_{sc}$  through,

$$V_{sc} = E_{sc} + R_{sc}I_{sc} \tag{33}$$

$$I_{sc} = C_{sc} \frac{dE_{sc}}{dt} \tag{34}$$

The grid-side converter circuit is utilized in adjusting the output power of DFIG and regulating DC bus voltage. Grid-side converter controls the terminal power of the

generator that supplies the reactive power the system requires. Reactive power reference is chosen as the reference value together with the AC bus voltage. Converter limits are counted in order to reach maximum reactive power compensation values. DC/DC converter and supercapacitor modeling in DFIG are shown in Fig. 2.

The difference between DC voltage and DC voltage reference enters proportional integral control, and the proportional limit value of the resulting signal is calculated based on minimum and maximum values. Limit value output is counted with d axis reference current. The supercapacitor circuit consists of four resistors and two capacitors. The capacitors that are used in capacity regulation control the system based on voltage. This capacity value is obtained based on the voltage equation supercapacitor capacity and applying interpolation to capacity–voltage curve in Fig. 3, both given in EPCOS catalogue [38, 39].

Voltage and voltage derivation of this curve are shown in Eqs. 35 and 36. As can be seen from the curve, the capacitance and voltage are proportional.

$$u_{LUP} = 7.1138 \times 10^{-8}t^3 + 1.1657 \times 10^{-3}t^2 + 6.4391t - 11945 \tag{35}$$

$$u_{LUP} = 2.13414 \times 10^{-7}t^2 + 2.3314 \times 10^{-3}t + 6.4391 \tag{36}$$

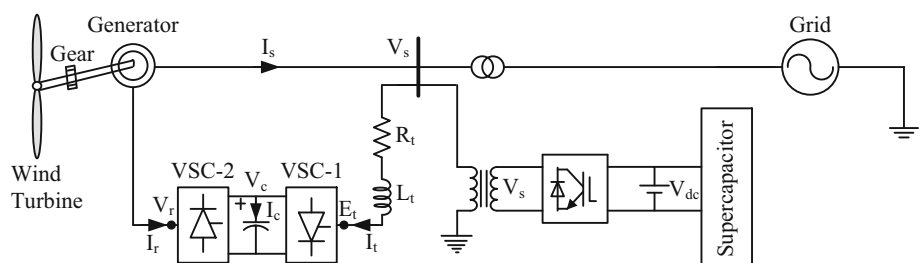
A buck–boost converter circuit is needed so that the voltage value produced in the supercapacitor equals to DC voltage value. Using the above curve, a capacity was determined based on the output voltage of the converters consisting of resistors, a coil, and a capacitor. Resistance value was determined based on the charge level of the supercapacitor in simulation.

The dynamics of output voltage ( $u_o$ ) and coil current ( $i_L$ ) in voltage boost converter circuit are defined as given in Eqs. 37 and 38, respectively.

$$\frac{du_o}{dt} = \frac{1}{C_0} \left[ (1 - D)i_L - \frac{u_o}{R_0} \right] \tag{37}$$

$$\frac{di_L}{dt} = \frac{1}{L_0} \left[ (1 - D)u_o - \frac{i_L}{R_0} \right] \tag{38}$$

**Fig. 1** DFIG and STATCOM-supercapacitor system configuration



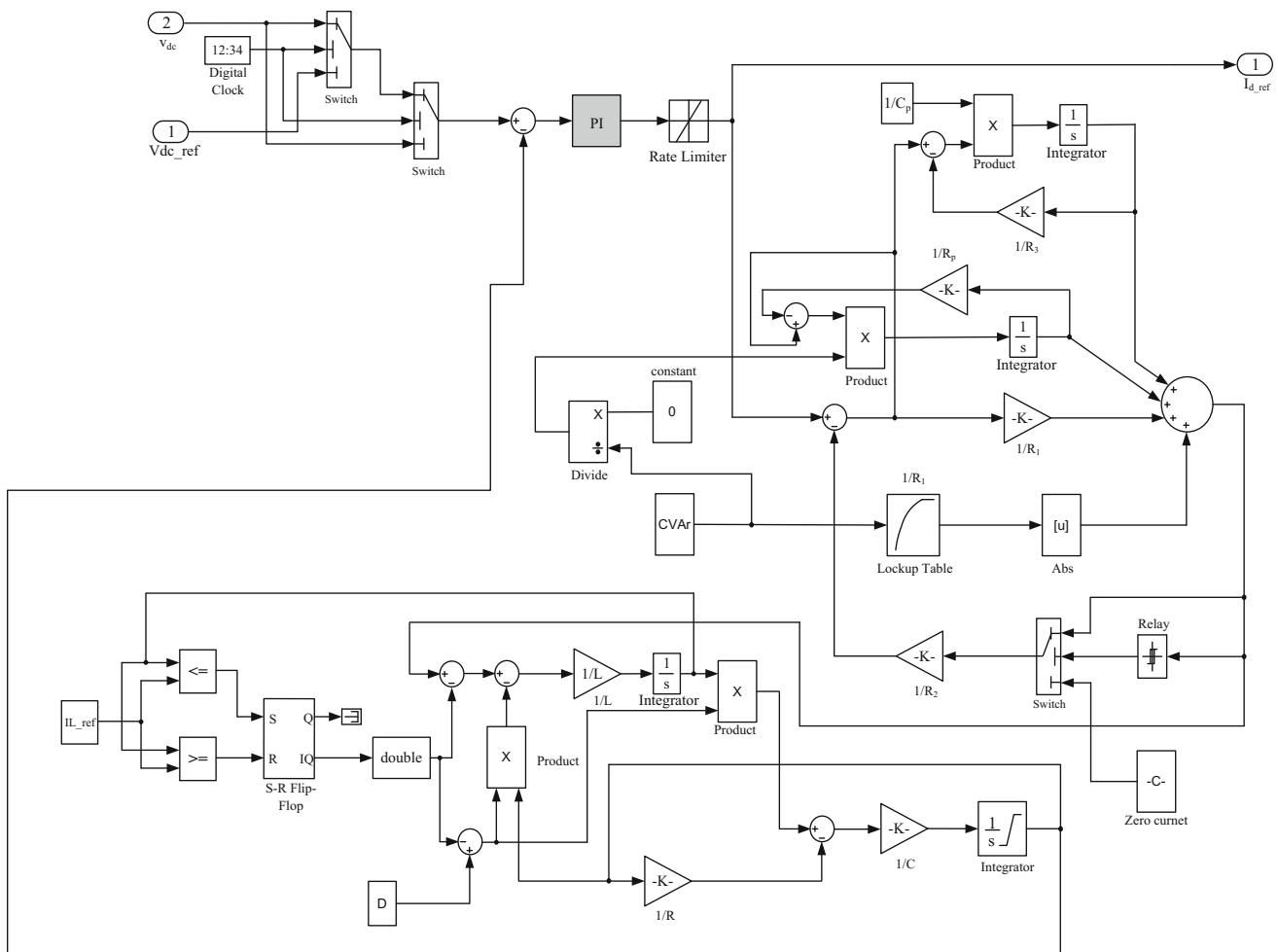


Fig. 2 DC/DC converter and supercapacitor modeling in STATCOM

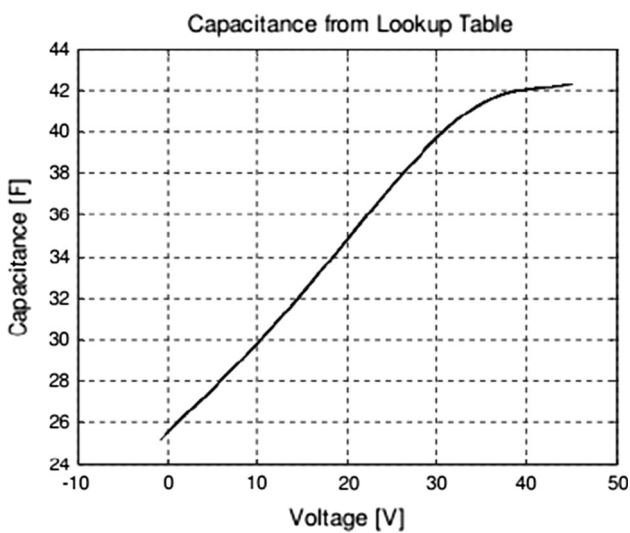


Fig. 3 Capacity–voltage curve of supercapacitor

### 5 Decoupled STATCOM-supercapacitor control

The supercapacitor-STATCOM system can be thought to float without having effects on any power flow to and from the supercapacitor when in steady state [40]. Figure 4 shows decoupled STATCOM-supercapacitor control.

The STATCOM operation is initiated by a variation through the steady condition, which can be detected through a change in generator output voltage magnitude and generator output voltage angle. STATCOM active and reactive power flows are given in Eqs. (39) and (40).

$$P_{st} = V_{st}I_{std} \cos \theta_s + V_{st}I_{stq} \sin \theta_s \tag{39}$$

$$Q_{st} = V_{st}I_{std} \sin \theta_s - V_{st}I_{stq} \cos \theta_s \tag{40}$$

The STATCOM current transforming is given in Eqs. (41) and (42).

$$I_{std}^{new} = I_{std} \cos \theta_s + I_{stq} \sin \theta_s \tag{41}$$

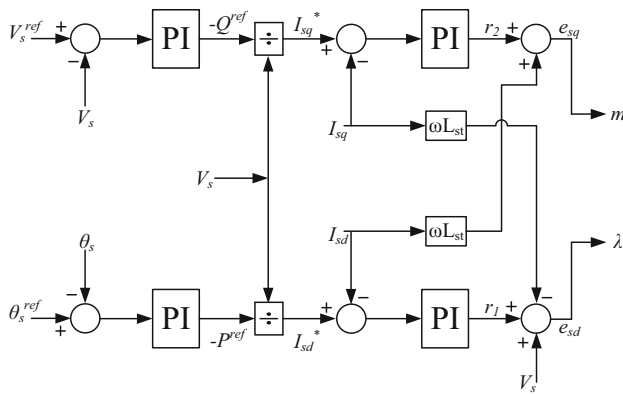


**Fig. 4** Decoupled STATCOM-supercapacitor control

$$I_{stq}^{new} = I_{std} \sin \theta_s - I_{stq} \cos \theta_s \tag{42}$$

Substituting Eqs. (41) in (42), the STATCOM active and reactive power can be achieved as Eqs. (43) and (44).

$$P_{st} = V_{st} I_{std}^{new} \tag{43}$$

$$Q_{st} = V_{st} I_{stq}^{new} \tag{44}$$

With the STATCOM currents being transformed from (41) and (42), Eqs. (30) and (31) can be achieved as Eqs. (45) and (46).

$$I_{std}^{new} = \frac{-R_{st}}{L_{st}} I_{std}^{new} + r_1 \tag{45}$$

$$I_{stq}^{new} = \frac{-R_{st}}{L_{st}} I_{stq}^{new} + r_2 \tag{46}$$

Here;

$$r_1 = w I_{stq}^{new} + \frac{m V_{dc}}{L_{st}} \cos \psi - \frac{v_s}{L_{st}} = w I_{stq}^{new} + \frac{e_{xd}}{L_{st}} - \frac{v_s}{L_{st}} \tag{47}$$

$$r_2 = -w I_{std}^{new} + \frac{m V_{dc}}{L_{st}} \sin \psi = -w I_{std}^{new} + \frac{e_{xq}}{L_{st}} \tag{48}$$

$$e_{xd} = L_{st} (r_1 - w I_{stq}^{new}) + v_s, e_{xq} = L_{st} (r_2 + w I_{std}^{new}) \tag{49}$$

$$m = \frac{\sqrt{e_{xd}^2 + e_{xq}^2}}{V_{dc}}, \psi = \tan^{-1} \left( \frac{e_{xq}}{e_{xd}} \right) \tag{50}$$

In Eqs. (45) and (46), transformed currents  $I_{std}$  and  $I_{stq}$  are excited by  $r_1$  and  $r_2$ , respectively.

### 6 Simulation study

System circuit modeling done simulation wind turbine-grid connection is given as detail in Fig. 5.

The wind turbine was a enhanced DFIG model with a STATCOM-supercapacitor, as explained in the previous Sect. 2 MVA power-rated STATCOM was connected to B

0.69-kV bus. The wind turbine was connected to a 34.5-kV system through a 0.85-MW, 0.69-kV Y/34.5-kV  $\Delta$  transformer. There was a distance of 1 km between the plant and the 34.5 kV grid. A 0.69 kV Y/34.5 kV  $\Delta$  transformer connected the transmission grid. The wind speed was considered as 8 m/s. The 34.5 kV grid-side short-circuit-powers was chosen as 2500 MVA, while the reactance/resistance rate was chosen as 7. In the DFIG, a stator resistance of 0.00706 ohm, rotor resistance of 0.005 ohm, stator inductance of 0.171 Henry, rotor inductance of 0.156 Henry and inertia constant of 3.5 s were chosen as the generator parameters.

### 7 Simulation study results

The impact of the STATCOM-supercapacitor on the system parameters was examined against two transient events. A 3-phase fault was considered as the first transient event. The fault was created in the middle of the transmission line in the time interval between 0.55 and 0.6 s. The variations in DFIG output voltage, active power, angular speed, electrical torque, and d–q axis stator current were observed for with and without STATCOM-supercapacitor. The comparisons of DFIG are shown in Fig. 6a–f.

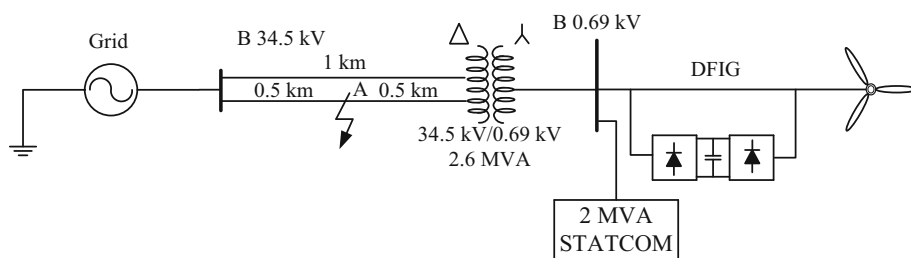
As can be seen from Fig. 6a, peak values of DFIG terminal voltage decreased and the system was stabilized in a shorter time, when STATCOM-supercapacitor is used. DFIG output voltage was around 0.32 p.u. with the use of supercapacitor in STATCOM, while it was 0.2 p.u. without supercapacitor in STATCOM. Moreover, oscillations in active power, angular speed, electrical torque, and d–q axes stator currents decreased very well with the use of the STATCOM-supercapacitor.

A two-phase fault was considered as the second transient event. The fault was created in the middle of the transmission line in the time interval between 0.55 and 0.6 s. The variations in DFIG output voltage, active power, angular speed, electrical torque, and d–q axes stator current were observed for the DFIG with and without the STATCOM-supercapacitor. The comparisons of DFIG are shown in Fig. 7a–f.

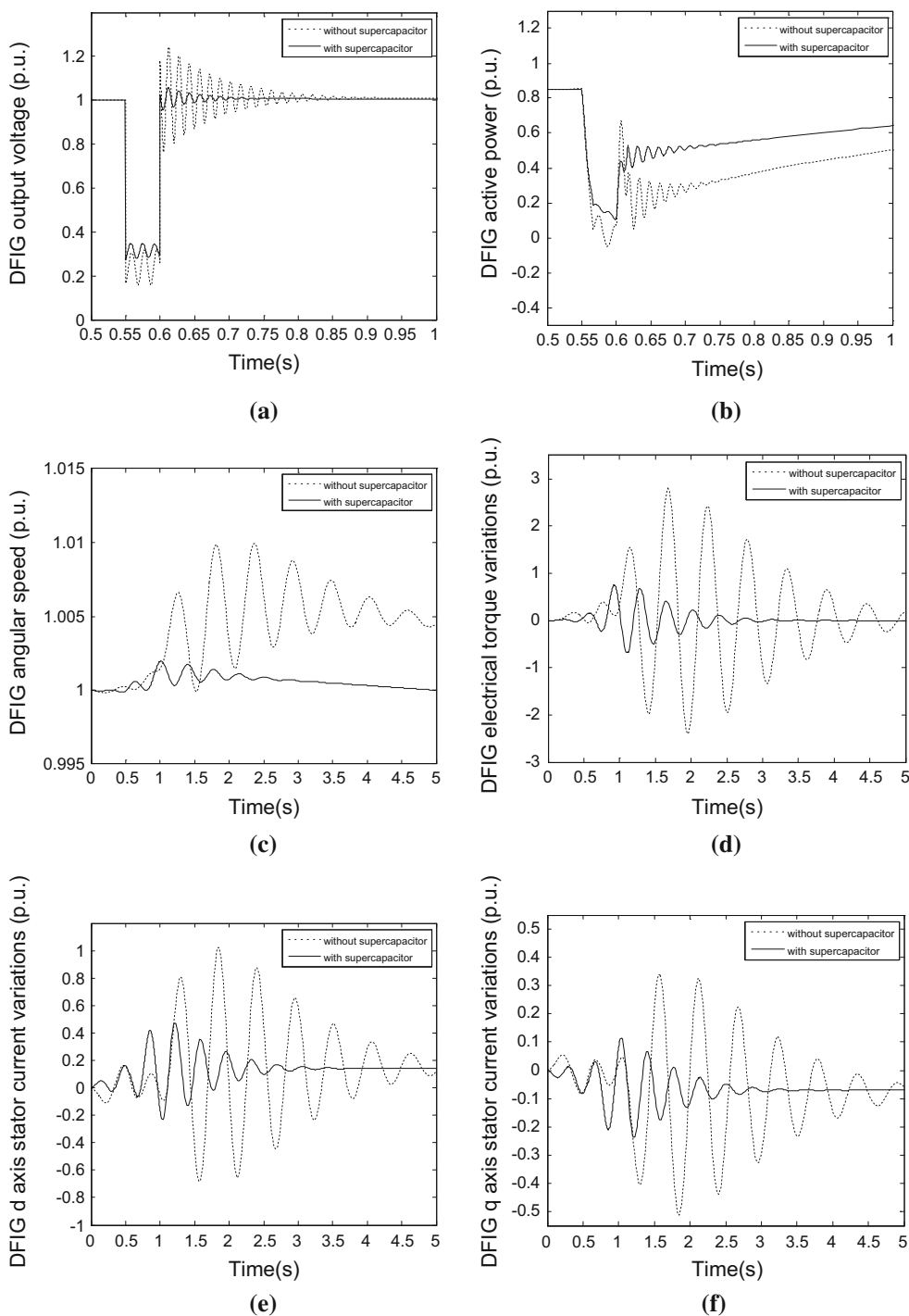
The results obtained from two-phase fault were shown on the same axes values as those of three-phase fault. DFIG terminal voltage is similar to the results obtained from three-phase fault; however, it was observed that oscillations were less. It was found that oscillation frequency was lower in two-phase fault in DFIG active power, DFIG angular speed, DFIG electrical torque, and d–q axes stator currents.

STATCOM reactive power variations during three-phase and two-phase fault are given in Fig. 8.

**Fig. 5** Test system



**Fig. 6** **a** DFIG output voltage (Three-phase fault), **b** DFIG active power (three-phase fault), **c** DFIG angular speed (three-phase fault), **d** DFIG electrical torque (three-phase fault), **e** DFIG d axis stator current variations (three-phase fault), **f** DFIG q axis stator current variations (three-phase fault)



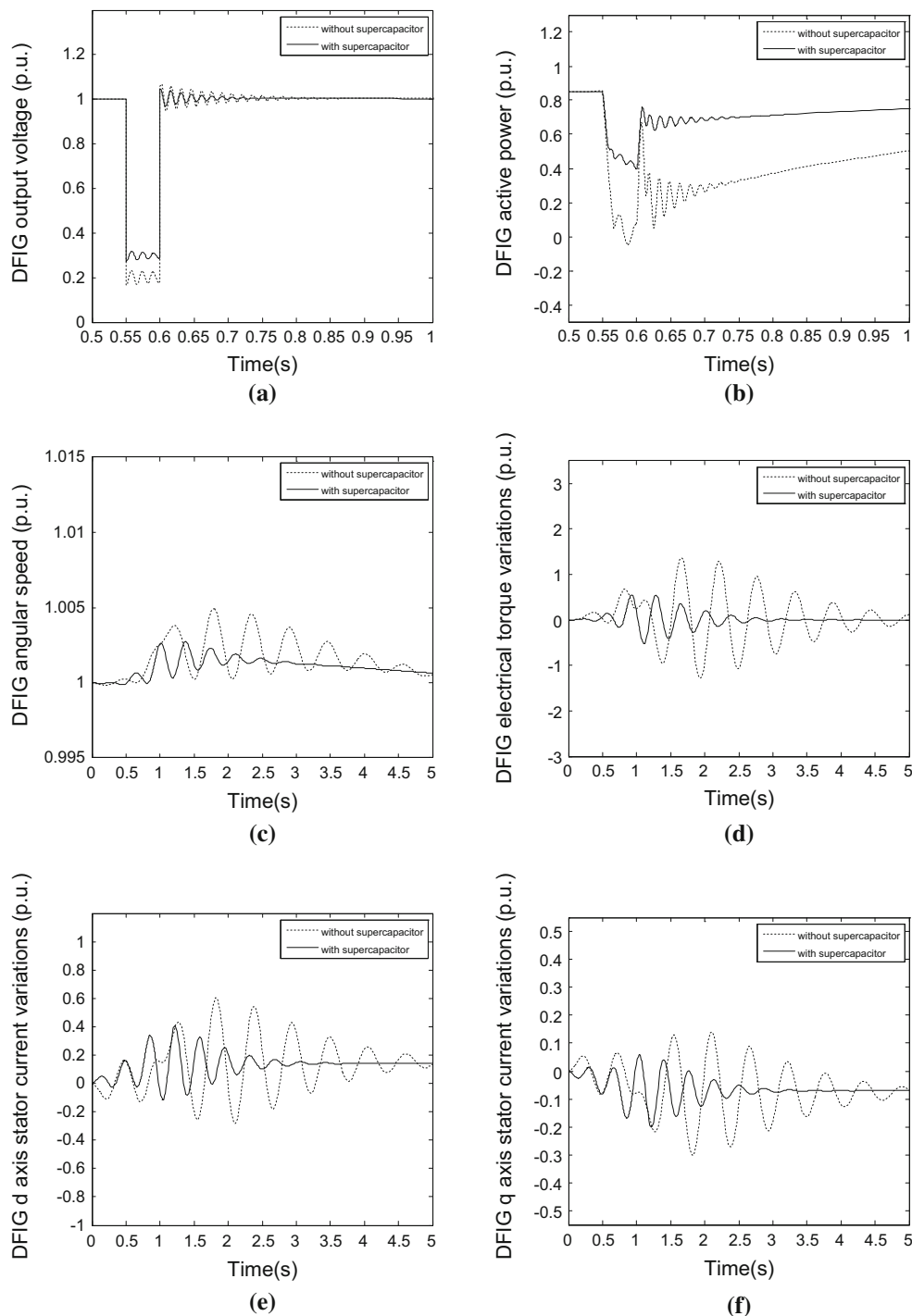


**Fig. 7** **a** DFIG output voltage (two-phase fault), **b** DFIG active power (two-phase fault), **c** DFIG angular speed (two-phase fault), **d** DFIG electrical torque (two-phase fault), **e** DFIG d axis stator

current variations (two-phase fault), **f** DFIG q axis stator current variations (two-phase fault)

## 8 Conclusion

This study presents an implementation of a STATCOM-supercapacitor energy storage system for a grid-integrated, DFIG-based wind farm. Modeling of the DFIG,

STATCOM-supercapacitor, and voltage buck–boost converter was carried out. The capacitance of the supercapacitor was determined by interpolation technique based on voltage–capacity relationship. The transient behaviors of the system with/without STATCOM-supercapacitor were



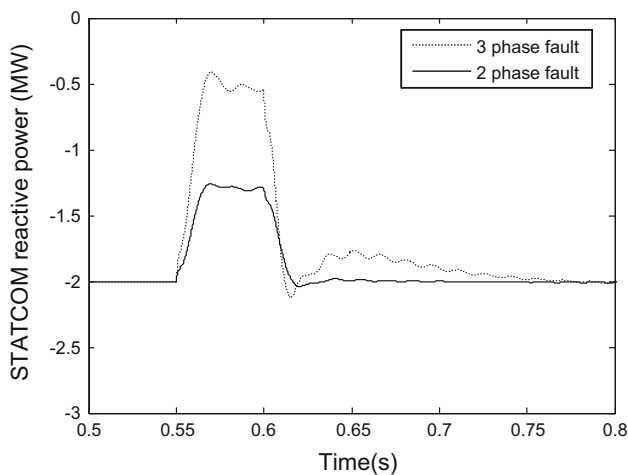


**Fig. 8** STATCOM reactive power variations

compared in terms of LVRT capability. Three-phase faults and two-phase fault for a short period of time were considered as transient events that may cause low voltage at the grid. Analysis results showed that oscillations observed after transient events were damped in a very short period of time with the use of supercapacitor energy storage system coupled to the STATCOM.

## References

- Hansen Anca D, Michalke Gabriele (2007) Fault ride-through capability of DFIG wind turbines. *Renew Energy* 32(9):1594–1610
- Seman S, Niiranen J, Arkkio A (2006) Ride-through analysis of doubly fed induction wind-power generator under unsymmetrical network disturbance. *IEEE Trans Power Syst* 21(4):1782–1789
- Gomis-Bellmunt O, Junyent-Ferre A, Sumper A, Bergas-Jan J (2008) Ride-through control of a doubly fed induction generator under unbalanced voltage sags. *IEEE Trans Energy Convers* 23(4):1036–1045
- Tsili M, Papathanassiou S (2009) A review of grid code technical requirements for wind farms. *IET Renew Power Gener* 3(3):308–332
- Canizares CA, Pozzi M, Corsi S, Uzunovic E (2003) STATCOM modeling for voltage and angle stability studies. *Elec Power and Energy Syst* 25(6):431–441
- Rao P, Crow ML, Yang Z (2000) STATCOM control for power system voltage control applications. *IEEE Trans Power Deliv* 15(4):1311–1317
- Qiao W, Venayagamoorthy GK, Harley RG (2009) Real-time implementation of a STATCOM on a wind farm equipped with doubly fed induction generators. *IEEE Trans Ind Electron* 45(1):98–107
- Muyeen SM, Takahashi R, Murata T, Tamura J (2010) A variable speed wind turbine control strategy to meet wind farm grid code requirements. *IEEE Trans Power Syst* 25(1):331–340
- Slepchenkov MN, Smedley K, Wen J (2011) Hexagram-Converter-Based STATCOM for voltage support in fixed-speed wind turbine generation systems. *IEEE Trans Ind Electron* 58(4):1120–1131
- Döğoğlu MK, Öztürk A (2012) Investigation of different load changes in wind farm by using FACTS devices. *Advanc in Eng Softw* 45(1):292–300
- Qiao W, Harley RG, Venayagamoorthy GK (2009) Coordinated reactive power control of a large wind farm and a STATCOM using heuristic dynamic programming. *IEEE Trans Energy Convers* 24(2):493–503
- Wang L, Hsiung CT (2011) Dynamic stability improvement of an integrated grid-connected offshore wind farm and marine-current farm using a STATCOM. *IEEE Trans Power Syst* 26(2):690–698
- Chen Z, Hu Y, Blaabjerg F (2007) Stability improvement of induction generator-based wind turbine systems. *IET Renew Power Gener* 1(1):81–93
- Han C, Huang AQ, Baran ME, Bhattacharya S, Litzemberger W, Anderson L, Edris A (2008) STATCOM impact study on the integration of a large wind farm into a weak loop power system. *IEEE Trans Energy Convers* 23(1):226–233
- Mohod SW, Aware MV (2010) A STATCOM-control scheme for grid connected wind energy system for power quality improvement. *IEEE Syst J* 4(3):346–352
- Molinas M, Suul JA, Undeland T (2008) Low voltage ride through of wind farms with cage generators: STATCOM versus SVC. *IEEE Trans Power Electron* 23(3):1104–1117
- Hossain MJ, Pota HR, Ramos RA (2011) Robust STATCOM control for the stabilization of fixed-speed wind turbines during low voltages. *Renew Energy* 36(11):2897–2905
- Kumar NS, Gokulakrishnan J (2011) Impact of FACTS controllers on the stability of power systems connected with doubly fed induction generators. *Elec Power and Energy Syst* 33(5):1172–1184
- Chatterjee D, Ghosh A (2011) Improvement of transient stability of power systems with STATCOM-controller using trajectory sensitivity. *Elec Power and Energy Syst* 33(3):531–539
- Wang L, Truong DN (2013) Stability enhancement of DFIG-based offshore wind farm fed to a multi-machine system using a STATCOM. *IEEE Trans Power Syst* 28(3):2882–2889
- Xiang D, Ran L, Bumby JR, Tavner PJ, Yang S (2006) Coordinated control of an HVDC link and doubly fed induction generators in a large offshore wind farm. *IEEE Trans Power Deliv* 21(1):463–471
- El-Moursi MS, Bak-Jensen B, Abdel-Rahman MH (2010) Novel STATCOM controller for mitigating SSR and damping power system oscillations in a series compensated wind park. *IEEE Trans Power Electron* 25(2):429–441
- Beza M, Bongiorno M (2015) An adaptive power oscillation damping controller by STATCOM with energy storage. *IEEE Trans Power Syst* 30(1):484–493
- Golshannavaz S, Mokhtari M, Nazarpour D (2011) SSR suppression via STATCOM in series compensated wind farm integrations. *IEEE 19th Iranian Electrical Engineering 2011 Conference* 1–6
- Knüppel T, Nielsen JN, Jensen KH, Dixon A, Østergaard J (2013) Power oscillation damping capabilities of wind power plant with full converter wind turbines considering its distributed and modular characteristics. *IET Renew Power Gener* 7(5):431–442
- Xu L (2008) Enhanced control and operation of DFIG-based wind farms during network unbalance. *IEEE Trans Energy Convers* 23(4):1073–1081
- Krause PC (2002) *Analysis of electric machinery*, 2nd edn. McGraw-Hill, New York
- Fernandez LM, Garcia CA, Jurado F (2008) Comparative study on the performance of control systems for doubly fed induction generator (DFIG) wind turbines operating with power regulation. *Energy* 33(9):1438–1452

29. Fernandez LM, Jurado F, Saenz JR (2008) Aggregated dynamic model for wind farms with doubly fed induction generator wind turbines. *Renew Energy* 33(1):129–140
30. Lobos T, Rezmer J, Sikorski T, Waclawek Z (2009) Power distortion issues in wind turbine power systems under transient states. *Turk J of Elec Eng Comput Sci* 16(3):229–238
31. Wu F, Zhang XP, Godfrey K, Ju P (2007) Small signal stability analysis and optimal control of a wind turbine with doubly fed induction generator. *IET Gener Transm and Distrib* 1(5):751–760
32. Díaz-González F, Sumper A, Gomis-Bellmunt O, Villafafila-Robles R (2012) A review of energy storage technologies for wind power applications. *Renew Sustain Energy Rev* 16:2154–2171
33. Zhao H, Wu Q, Hu S, Xu H, Rasmussen CN (2015) Review of energy storage system for wind power integration support. *Appl Energy* 137:545–553
34. Abbey C, Joos G, (2005) Short-term energy storage for wind energy applications. *IEEE Fourtieth IAS Industry Applications Conference, 2005, Montreal, Canada*, pp. 2035–2042
35. Abbey C, Joos G, (2005) Effect of low voltage ride through (LVRT) characteristic on voltage stability. *IEEE Power Engineering Society General Meeting, 2005, Varennes, Canada*, 1901–1907
36. Slootweg JG, Polinder H, Kling WL (2001) Dynamic modelling of a wind turbine with doubly fed induction generator. *IEEE Power Eng Soc Summer Meet* 1:644–649
37. Rahim AHMA, Nowicki EP (2012) Supercapacitor energy storage system for fault ride-through of a DFIG wind generation system. *Energy Convers and Manage* 59:96–102
38. Data sheet for supercapacitor from EPCOS with part no.: B48621-S0203-Q288
39. Gaiceanu M (2012) MATLAB/simulink-based grid power inverter for renewable energy sources integration, *MATLAB-A Fundamental Tool for Scientific Computing and Engineering Applications*. 1–219
40. Alam MA, Rahim AHMA, Abido MA (2010, July) Supercapacitor based energy storage system for effective fault ride through of wind generation system. *Industrial electronics (ISIE), 2010 IEEE international symposium, Bari, IEEE*. 2481–2486